THE ASTROPHYSICAL JOURNAL, 485:100–111, 1997 August 10

HUBBLE SPACE TELESCOPE OBSERVATIONS OF THE GRAVITATIONALLY LENSED CLOVERLEAF BROAD ABSORPTION LINE QSO H1413+1143: IMAGING[1]

DAVID A. TURNSHEK,[2] OLIVIA L. LUPIE,[3] SANDHYA M. RAO,[2]
BRIAN R. ESPEY,[4] AND CHRISTOPHER J. SIROLA[2,5]
Received 1996 August 15; accepted 1997 February 27

ABSTRACT

An analysis of *Hubble Space Telescope* (*HST*) Wide Field Planetary Camera (WFPC) and Wide Field Planetary Camera 2 (WFPC2) images of the gravitationally lensed Cloverleaf broad absorption line quasi-stellar object (QSO) H1413+1143 is presented. Astrometric and photometric measurements are derived for the four components of the lensed QSO for five different epochs over a baseline of 2.76 yr. Because of the replacement of WFPC with WFPC2 and the change in the purpose of the observation at the various epochs, the data were not always taken with the same filter. With the exception of the declination of component D, the relative positions of the four components are measured to within ≈ 3 mas; these results are consistent with but considerably more accurate than earlier measurements. The relative photometric measurements at any one epoch are typically accurate to ≈ 0.02–0.03 mag (1 σ). The initial *HST* WFPC images cover a baseline of 1.26 yr (1992.21–1993.47 [1992 March 16–1993 June 22]), and over this time interval there is little evidence for brightness variations of any of the components relative to one another at levels > 0.06 mag ($> 2\ \sigma$). Photometric measurements of the more accurate WFPC2 data obtained with different filters extends this baseline an additional 1.50 yr (to 1994.97 [1994 December 22]). The WFPC2 data also fail to reveal significant brightness variations among the components. In addition, the WFPC2 data include both UV (F336W) and near-infrared (F814W) images. These color data indicate the presence of sight-line–dependent extinction, causing the F336W–F814W color index of component B (the most reddened component) to be 0.56 ± 0.04 mag redder than that of component C (the least reddened component). The lack of evidence for significant component brightness variations at all *HST* observation epochs suggests that the data could be reliably extinction-corrected to derive the relative amplifications of the four image components. This is done for several reasonable dust-extinction models. Thus, the derived astrometry along with the photometric analysis set clear constraints on models for the Cloverleaf. Since component D shows some evidence for microlensing, the results on its relative amplification should be used with caution. While existing models can successfully reproduce the relative positions, the relative amplifications have not yet been successfully modeled.

The WFPC2 imaging data has also permitted a sensitive search for component structure and the gravitational lens itself. There is marginal evidence for elongated structure between components A and C that may be part of an Einstein ring. However, no significant evidence for the lensing object is found. The various measurements are quantified in ways useful for setting model constraints. Limits on the mass-to-light ratio and detectability of the lensing galaxy are also discussed.

Subject headings: astrometry — galaxies: photometry — gravitational lensing — quasars: individual (QSO H1413+1143)

1. INTRODUCTION

The quasi-stellar object (QSO) H1413+1143 ($m_V \approx 17$) was discovered by Hazard et al. (1984) in an objective prism plate survey. A distinguishing characteristic of the object's spectrum was the presence of broad absorption lines (BALs). Magain et al. (1988) later found that H1413+1143 was a gravitationally lensed system with four visible components. Surdej (1990) and Angonin, Vanderriest, & Surdej (1990) confirmed that the spectra of the four components were strikingly similar, all having an emission redshift of $z_{em} \approx 2.5$ and BALs. All four components fall within 0.″6 of the image center (Magain et al. 1988), and the name "Cloverleaf" was adopted because of its four-leaf-clover–like configuration and the similar brightnesses of the components. Kayser et al. (1990) have shown that a close correlation exists between the Cloverleaf's weak radio structure and its optical properties, and they have presented example gravitational lens models for the system. Ground-based observations have not led to the detection of the lensing object, nor have they led to the detection of any plausible additional components. We present here the results of sensitive *Hubble Space Telescope* (*HST*) Wide Field Planetary Camera (WFPC) and Wide Field Planetary Camera 2 (WFPC2) observations, but we have also been unable to find significant evidence for any lensing object, although we have found some evidence for additional component structure. With these new observations we are able to derive more accurate results on the relative locations of the image components and their relative amplifications. Moreover, we are able to place sensitive photometric con-

[1] Based on observations with the NASA/ESA *Hubble Space Telescope*, obtained at the Space Telescope Science Institute, which is operated by AURA, Inc., under NASA contract NAS 5-26555.

[2] Department of Physics and Astronomy, University of Pittsburgh, Pittsburgh, PA 15260.

[3] Computer Science Corporation and Space Telescope Science Institute, 3700 San Martin Drive, Baltimore, MD 21218.

[4] Department of Physics and Astronomy, Johns Hopkins University, Baltimore, MD 21218.

[5] Present address: Tri-County Technical College, Clemson, SC 29634.

straints on the brightness of any lensing object and additional component structure.

The existence of a gravitationally lensed BAL QSO with this particular type of geometry is very significant because, by obtaining spectroscopy of the individual components, the emission-line region (e.g., Saust 1994), the sizes and shapes of BAL region structures (e.g., Hutsemekers 1993), and the sizes and shapes of intervening narrow absorption-line clouds can be studied (e.g., Smette et al. 1995). For the Cloverleaf, these topics are the subject of additional papers (Turnshek et al. 1997; Monier, Turnshek, & Lupie 1997), and only results derived from *HST* imaging are considered here. Reviews and references to recent work on BAL QSOs can be found elsewhere (e.g., Weymann, Turnshek, & Christiansen 1985; Turnshek 1988, 1995; Turnshek et al. 1994; Turnshek 1995; Weymann 1995). The astrometry and photometry of the four image components and searches for component structure and the gravitational lens itself are described in § 2. *HST* imaging constraints on the model of the lens are considered in § 3. A summary and discussion of the work are given in § 4.

2. *HST* WFPC AND WFPC2 IMAGING OF THE CLOVERLEAF

The journal of *HST* imaging observations is presented in Table 1. The observations took place at five different epochs, and in all cases the data were taken in planetary camera (PC) mode. The 800 pixel × 800 pixel field of view of the PC is 33″ × 33″ for the WFPC and 36″ × 36″ for the WFPC2. Each data set is useful for deriving accurate relative astrometry and photometry. To obtain the WFPC data (with spherically aberrated images), two exposures were taken through the F555W filter on PC 6 at each of three different epochs: 1992 March 16 (1992.21, archival data), 1992 May 2 (1992.33), and 1993 June 22 (1993.47). Unfortunately, only one of the two images takens on 1992.21 was of reasonable quality because of poor tracking throughout the exposures, and a spurious noise event on 1993.47 contaminated one of the two images near component A. To obtain the WFPC2 data (with post–*HST*-servicing-mission corrective optics in place), a number of multiple exposures were taken through various filters at two epochs. On 1994 July 11 (1994.53) five F702W exposures and three F255W exposures were taken. The F255W images were essentially blank; we later determined that this was almost certainly due to a strong intervening Lyman limit absorption edge that set in longward of the effective red edge of the filter, obscuring all four of the image components (Monier et al. 1997). On 1994 December 22 (1994.97) three F814W exposures, two F702W exposures, and three F336W exposures were taken. These latest data are useful for considering sight-line–dependent extinction (§ 2.2.4), which is present and affects the apparent relative component amplifications in all optical filters.

In Figure 1 (Plate 1) we present an F814W image (*upper left*) an F336W image (*upper right*) a color rendition of the combined F336W and F814W data (*lower left*), and the sum of the three 15 minute F702W exposures in which the contrast has been adjusted to reveal low surface brightness features (*lower right*). The lower left-hand image is presented in color because it nicely illustrates the sight-line–dependent extinction (see § 2.2.3 and the figure legend). A two-dimensional intensity histogram of one of the WFPC2 PC observations is shown at the top of Figure 2. The resolution in the WFPC2 PC mode was measured to be typically ≈0.″08 (core FWHM).

2.1. *Astrometry of the Cloverleaf Components*

Relative astrometric measurements of the image components were made by fitting two-dimensional Gaussian profiles to each component to determine their centers. The positions of the components on the CCD were then converted to right ascension and declination while accounting for the geometric distortions of the chip. Distortion corrections accounted for errors less than 0.1 pixels (<4 mas) in the individual component positions. The accuracies of the WFPC and WFPC2 relative astrometry are ≈7 mas and ≈3 mas, respectively. With the exception of the measurement of the relative declination of component D, there is no evidence for shifts in the relative positions of the components at the five observation epochs. The combined results from all the observations are reported in Table 2, with a comment on the relative declination of component D in a footnote to the table. Thus, the overall results are generally accurate to ≈3 mas. These results represent an improvement over earlier ground-based measurements by more than a factor of 3 and are consistent with them (Magain et al. 1988; Kayser et al. 1990). Accurate astrometry can play an important role in deriving accurate relative photometry (see §§ 2.2.1 and 2.2.2), and therefore ground-based photometry of the Cloverleaf should benefit from this increased accuracy.

2.2. *Photometry of the Components of the Lensed QSO*

Photometry of starlike images using *HST* is different than ground-based photometry in several important ways. First, the atmosphere does not play a role in determining

TABLE 1

JOURNAL OF *HST* WFPC AND WFPC2 IMAGING OBSERVATIONS OF THE CLOVERLEAF

Date	PC2 Mode	Exp Time (s)
1992 Mar 16 (1992.22)[a]	PC2 F555W	100, 900
1992 May 02 (1992.33)	PC2 F555W	2 × 300
1993 Jun 22 (1993.47)	PC2 F555W	2 × 500
1994 Jul 11 (1994.53)	PC2 F702W	2 × 100, 3 × 900
	PC2 F255W[b]	3 × 800
1994 Dec 22 (1994.97)	PC2 F814W	3 × 300
	PC2 F702W	2 × 200
	PC2 F336W	3 × 900

[a] Archival data.
[b] Blank frames, likely due to intervening Lyman limit absorption.

TABLE 2

COMPONENT POSITIONS RELATIVE TO COMPONENT A IN THE CLOVERLEAF

Component	ΔR.A. (err) (arcsec)	Δdecl. (err) (arcsec)
A	0.000 (...)	0.000 (...)
B	0.744 (0.003)	0.172 (0.003)
C	−0.491 (0.003)	0.716 (0.004)
D	0.355 (0.003)	1.043 (0.012)[a]

[a] The WFPC and WFPC2 measurements of component D's declination are significantly different. The WFPC value taken at a mean epoch of 1992.7 is 1.063 ± 0.007, while the WFPC2 value taken at a mean epoch of 1994.8 is 1.038 ± 0.003.

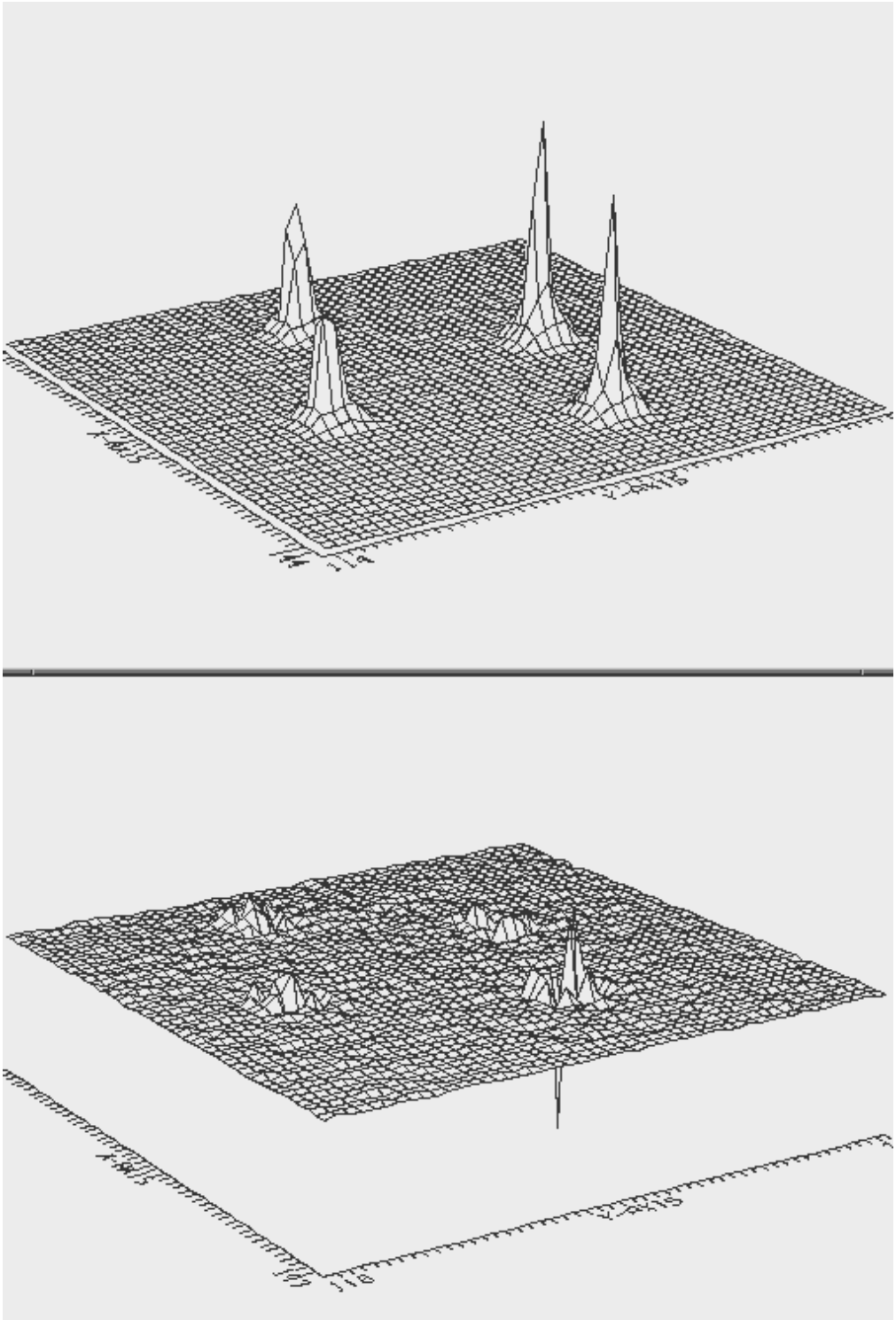

FIG. 2.—The top panel shows a two-dimensional intensity histogram of a portion of one of the 200 s WFPC2 F702W images taken on 1994.53. This illustrates the resolution in the WFPC2 PC mode, which has a measured FWHM $\approx$ 0.08 arcsec $\approx$ 2 pixels. The bottom panel shows the PSF-subtracted result. The cores of the four components appear to subtract poorly because of imperfect registration and slight undersampling. The noise within the subtracted regions is consistent with the background and is higher in regions where the PSFs overlap.

extinction or seeing conditions. Also, the "sky" background is darker. The WFPC F555W filter used in some of the observations is roughly similar to the familiar ground-based Johnson *V* band, the WFPC2 F336W filter is similar to the Johnson *U*, the WFPC2 F702W filter represents a wide *R* band, and the WFPC2 F814W filter is similar to the Cousins *I*. As the WFPC F555W data were taken before the *HST* servicing mission, the severe image aberrations in these data make it especially necessary to adopt techniques used to obtain photometry in crowded fields. In the aberrated images, only $\approx$12% of the light from a point source is contained within the central 3 pixels, and the outer envelopes of the point-spread functions (PSFs) overlap and extend out to more than 1″. Other effects that limit the

accuracy of WFPC photometry are discussed in Phillips et al. (1994).

Because of the difficulties of working with spherically aberrated images, we have used two independent methods for obtaining relative magnitudes of the QSO image components from WFPC data (§§ 2.2.1 and 2.2.2). Using more than one method allowed us to check the robustness of the techniques and assess the limitations of WFPC photometry in crowded fields. However, it was adequate to consider only one method to derive results from the WFPC2 photometry (§ 2.2.3), although these data still have limitations (Holtzman et al. 1995b). Results from the WFPC2 photometry lead to F336W–F814W color indices for the four components that reveal the presence of sight-line–dependent extinction (§ 2.2.4). We also derive the apparent magnitude of the Cloverleaf system as a whole in various filters at the different epochs and assign apparent magnitudes to each of the components (§ 2.2.5). We then summarize the main conclusions that can be derived from the photometric measurements (§ 2.2.6).

The results are consistent with the more limited results reported by Falco (1993), which were based on some WFPC F555W data.

2.2.1. *WFPC Relative Magnitude Measurements Using a Core-Subtraction Technique*

One algorithm that was utilized to measure WFPC F555W images involved modeling the cores of each component separately (defined as being within the central 3 pixels, or $\approx 0\farcs13$) with artificial PSFs and then combining all four PSFs to make a model of the Cloverleaf. Specifically, the model parameters were adjusted to approximate the measured photometry of the image within the cores by the following procedure.

Artificial PSFs were derived using the Tiny Tim software package developed by Krist (1993) specifically for *HST* data. The package generates an artificial PSF by considering the date of the observation, the CCD detector used, the pixel position of the image on the CCD, the filter used, the approximate extent of the image ($\approx 1''$), and the estimated telescope jitter (≈ 15 mas, as is usually the case). The number of counts in each artificial PSF was made equal to the number of counts measured in the components' cores on the image to be modeled, and the component locations were set equal to the measured ones (§ 2.1). All four adjusted PSFs were then combined into a single image to model the entire Cloverleaf. The photometry of the system could then be estimated. The results from this model were then used to create a more accurate model, and the procedure was repeated. This iterative process was used to adjust the brightnesses of each PSF so that the photometry of the model matched the actual images within the component cores. Usually no more than five iterations were needed for convergence.

Except for the 1993.47 measurements of component A, which is contaminated by a spurious noise event, this process results in differential photometry with an accuracy of ≈ 0.03–0.05 mag. The results are presented in Table 3. The primary drawback of this method is that the shapes of the artificial PSFs do not precisely match those in the observed images, especially in the wings. Another difficulty is that an error of ≈ 10 mas in the position of one of the components can result in a change of ≈ 0.02 mag, effectively increasing the uncertainty of the measurement. Thus, errors in astrometric measurements that are not too different from the actual errors can significantly limit the photometric accuracy. The errors reported in Table 3 are estimates based on comparing the photometry derived independently from the two separate images that were taken on each observation date.

TABLE 3

WFPC F555W Relative Photometry of the Cloverleaf Components with the Core-Subtraction Method[a]

	Δmag (err)		
Component	1992.21	1992.33	1993.47
A	−0.22 (...)[b]	−0.28 (0.05)	−0.34 (0.07)[a]
B.....	−0.06 (...)[b]	−0.07 (0.03)	−0.03 (0.01)
C	0.00 (...)[b]	0.00 (...)	0.00 (...)
D	0.06 (...)[b]	0.15 (0.03)	0.14 (0.03)

[a] Measurements are presented relative to component C because of the spurious noise event that occurred near component A on 1993.47 and because component C is the least reddened.

[b] Poor tracking precluded using the core-subtraction method on one of the two observations obtained on this date; therefore, estimated errors are not reported.

2.2.2. *WFPC Relative Magnitude Measurements Using LUCY Image Restoration*

The second algorithm that was utilized for photometry of WFPC F555W images is one that makes use of the LUCY restoration method and the known morphology of the object under study (Lucy 1971; Houde & Racine 1994). Because the positions of the four components are well known and their magnitudes are roughly equal, a workable first estimate of the solution can be specified, something not ordinarily possible. A measurement was accomplished by first using artificial PSFs to simulate the image (see § 2.2.1). The PSF tht was used for the restoration itself was also artificially generated and centered at the geometric mean position of the Cloverleaf. For simplicity, each PSF used in the initial estimated image was given the same brightness; changing the brightnesses of the PSFs used in the initial image made no significant difference in the results. Also, the astrometry is accurate enough to guarantee that, for this technique, no significant errors in photometry are caused by astrometric errors. In all cases, convergence was rapid, and the restored image components did not have extended envelopes.

This method was more consistent for frames taken on the same date than was the core-subtraction method. Except for the 1993.47 measurement of component A, which remained problematic, comparison of separate frames indicates that this technique results in differential photometry that has an accuracy of ≈ 0.02–0.03 mag. The results from this method are reported in Table 4.

2.2.3. *WFPC2 Relative Magnitude Measurements*

The Cloverleaf was observed with *HST* through the WFPC2 F255W, F336W, F702W, and F814W filters. See Table 1 for the details. The cores of all four components in the three 900 s F702W images were saturated; these images were used to search for evidence of additional component structure and the lensing object (§ 2.3). WFPC2 F702W magnitudes on 1994.53 were determined from the two 100 s exposures. The F255W frames were blank, almost certainly because of an intervening Lyman limit absorption system. Of the three F336W frames, one was severely contaminated

TABLE 4

WFPC F555W Relative Photometry of the Cloverleaf Components with the LUCY Restoration Method[a]

	Δmag (err)		
Component	1992.21	1992.33	1993.47
A	−0.23 (0.01)	−0.26 (0.01)	−0.36 (0.08)[a]
B.....	−0.06 (0.01)	−0.02 (0.01)	−0.04 (0.02)
C	0.00 (...)	0.00 (...)	0.00 (...)
D	0.08 (0.03)	0.17 (0.01)	0.13 (0.02)

[a] Measurements are presented relative to component C because of the spurious noise event that occurred near component A on 1993.47 and because component C is the least reddened.

by a cosmic-ray streak whose height was ≈10 times that of the individual components and cut across the center of the Cloverleaf. This frame was not used to measure F336W magnitudes. The procedure described below was used to determine the relative magnitudes of the four components through all filters. The results are presented in Table 5.

The magnitudes of isolated stars can be determined accurately using aperture photometry, i.e., a simple measurement of counts within a defined aperture. However, the four components of the Cloverleaf are separated by less than an arcsecond, and the wings of the PSFs of the four point sources overlap to some extent even with the *HST*-WFPC2 corrective optics. Thus, we are still dealing with a crowded field. In this situation, the best approach would have normally been to determine the PSF from an isolated point source in the same frame as the Cloverleaf and to fit it to the four components simultaneously. Not only would this yield accurate magnitudes, but subtraction of the fit from the original frame might reveal additional component structure or the lensing object. However, the fits obtained with the archived PSFs were not satisfactory. Since the PC frames have no other point sources, the Cloverleaf components themselves were used to model the PSF. Tasks in the IRAF[6] DAOPHOT software package were used to determine a PSF for each frame using one or more of the Cloverleaf components as the "PSF stars." Specifically, the tasks DAOFIND and PHOT were used to obtain preliminary estimates of the magnitudes of the four components. Then, the tasks PSF and NSTAR were used to model the PSF and fit the model to the four components. The four components were placed in groups based on suitably chosen parameters such as the radius of the PSF and the distance between components. For example, component D is farthest away from the other three; hence, components A, B, and C were placed in one group, while component D was in a group by itself. The profiles of components belonging to the same group were then fit simultaneously. The output of NSTAR consisted of improved magnitudes and errors. The errors in magnitudes included errors due to Poisson noise, readout noise, flat fielding, and profile fitting. Details on these tasks are available through on-line help pages and IRAF documentation.

The goodness of fit was determined in two ways. First, the task NSTAR calculates a goodness-of-fit statistic, χ, which is the ratio of the observed pixel-to-pixel scatter in the fitting residuals to the expected scatter (determined from the four error contributors listed above). A good fit would result in $\chi \approx 1$. We obtained χ-values for the four components that scattered around unity in all frames. Second, we visually inspected the residuals by subtracting the fit from the original frame. Examples of original and subtracted frames are shown in Figure 2. The cores of the four components subtracted poorly because of registration and undersampling problems (the FWHM of the core was somewhat less than 2 pixels in all frames). However, the magnitudes derived were in agreement with the results from aperture photometry, confirming that the quality of the core subtraction did not affect the fitted magnitudes. We performed several consistency checks to verify the accuracy of the derived magnitudes. Figure 2 shows that the noise within the subtracted regions is consistent with the background and, as expected, is higher in regions where the PSFs overlap.

Note that the subtracted image shown at the bottom of Figure 2, which is a short exposure frame, does not show any obvious underlying structure. However, an important concern is that any underlying structure might be included in the modeled PSF and thus might be subtracted out. Any significantly bright structure associated with one or more of the point sources would have shown up in the modeled PSF (if the extended component was picked as the "PSF star") or in the subtracted image (if the extended component was not a PSF star). No evidence for structure resulted from either possibility. In § 2.3 we discuss extended structure, and place upper limits on the magnitude of the lensing galaxy at positions of interest.

According to Holtzman et al. (1995b), several corrections may need to be applied to measurements taken from the WFPC2 PC CCD (see also Whitmore 1995). (1) Charge transfer efficiency effects are important. The WFPC2 CCDs have a charge transfer efficiency problem that causes some signal to get lost as the charge is transferred during readout.

[6] IRAF is distributed by NOAO, which is operated by AURA, Inc., under contract to the NSF.

TABLE 5

WFPC2 Relative Photometry of the Cloverleaf and Its Components[a]

	Δmag (err)				
Component	PC2 F702W (1994.53)	PC2 F814W (1994.97)	PC2 F702W (1994.97)	PC2 F336W (1994.97)	F336W–F814W (1994.97)
A	−0.31 (0.04)	−0.30 (0.03)	−0.28 (0.02)	0.02 (0.04)	0.32 (0.05)
B.....	−0.14 (0.04)	−0.20 (0.03)	−0.13 (0.02)	0.36 (0.02)	0.56 (0.04)
C	0.00 (...)	0.00 (...)	0.00 (...)	0.00 (...)	0.00 (...)
D	0.10 (0.04)	0.09 (0.03)	0.07 (0.02)	0.19 (0.04)	0.10 (0.05)

[a] Measurements are presented relative to component C for ease of comparison with Tables 3 and 4 and because component C is the least reddened.

The required correction was reduced from an ≈10%–15% gradient in counts from the bottom to the top of the CCD to a maximum 4% gradient after the cooldown date, 1994 April 23, when the CCD operating temperature was changed from −76 to −88 C. Holtzman et al. (1995a) determined that the effect was background dependent and recommended a correction of a 4% ramp for low background levels. The data here were taken at the lower operating temperature, had little background, and were at the center of the CCD. We therefore applied a 2% correction to the counts in all four components of all the images. (2) The time dependence of the UV throughput is also important. The CCDs accumulate contaminants over a period of time. The effect on throughput is negligible in the infrared and visible, but can be dramatic in the UV. The CCDs are decontaminated (warmed up) once a month, a process that completely restores UV throughput. The loss in throughput between decontaminations is linear, and a simple linear interpolation between decontamination dates corrects for this effect. The correction is given by

$$m_{\rm true} = m_{\rm obs} + dt \ ,$$

where $m_{\rm obs} = -2.5 \times \log ({\rm DN}/s)$, DN is the data number as read from the CCD, s is the exposure time in seconds, d is the rate of contamination, and t is the number of days since the last decontamination. The UV data were obtained with the PC through the F336W filter at the operating temperature of −88 C and were taken 4 days after decontamination. For these specifications $d = 0.0007 \pm 0.0005$ (Holtzman et al. 1995b). Therefore, the observed F336W magnitudes were corrected by 0.003 ± 0.002 magnitudes. (3) The pipeline processing should be assessed. We found the pipeline processing to be nominal and therefore adequate. We have not reprocessed the data using calibration frames that were taken at times nearest to the observation dates because this was unnecessary. (4) Aperture corrections were made. The PSF of a diffraction-limited image essentially extends out to infinity. Therefore, point-source photometry must be defined within a specific aperture size. Holtzman et al. (1995b) used an aperture of 0.″5 radius for all their photometric calibration measurements. We used their measurements to calibrate ours and therefore selected an aperture size of the same radius, which for the PC is 11 pixels. Had we used an aperture of a different size, we would have had to correct the measurements as described in Holtzman et al. (1995a). Appropriate zero points were then used to derive apparent magnitudes (see § 2.2.4). Note that the background within an aperture contributed by the other three PSFs is properly subtracted by the DAOPHOT routines described above. (5) Geometric distortion was assessed and found to be unimportant. The four components of the Cloverleaf lie near the center of the CCD in all the frames. Geometric distortion in this region is less than 0.2% (Holtzman et al. 1995a), and it was not necessary to apply a correction for photometry.

2.2.4. *Evidence for Sight-Line–dependent Extinction*

The last column of Table 5 gives the F336W − F814W color for the four components. component B (the most reddened component) is 0.56 ± 0.04 mag redder than component C (the least reddened component). Components A and D are ≈0.32 mag and ≈0.10 mag redder than component C, respectively. The differences in color along the four sight lines are present at a high level of significance and are shown graphically in Figure 3. Reasonable models for the sight-line–dependent extinction are considered in § 4.

2.2.5. *Derivation of Apparent Magnitudes Using Synthetic Photometry*

To put measured count rates on an apparent magnitude scale, the photometry of the Cloverleaf had to be modeled by considering the detector-filter combination used and the expected spectral dependence of the object of interest. A flat spectrum in f_λ is a reasonable approximation for the Cloverleaf over the filter wavebands of interest (e.g., see the spectra of Drew & Boksenberg 1984; Turnshek et al. 1988, 1997; and Monier et al. 1997). We decided to use the STMAG system and appropriate zero points because it relates the observed flux to magnitudes for a constant f_λ spectrum (Holtzman et al. 1995b). In this system, an object with a flat f_λ spectrum and $m = 0$ will have a monochromatic flux of 3.63×10^{-9} ergs s^{-1} cm^{-2} Å^{-1}. The STMAG is given by

$$\text{STMAG} = -2.5 \times \log ({\rm DN}/s) + Z_{\rm STMAG} + 2.5 \log {\rm GR} \ ,$$

where again DN is the data number as read from the CCD and s is the exposure time in seconds, $Z_{\rm STMAG}$ is the STMAG zero point for the filter of interest (given in Table 9 of Holtzman et al. 1995b), and GR is the gain ratio, as explained below. WFPC2 data can be read out through either of two available gain states. The calibration frames that were used to flat-field the data were taken with a gain of $\approx 14e^-$/DN, while the science data were taken with a gain of $\approx 7e^-$/DN. More precisely, this gain ratio for the PC is GR = 1.987. In addition, the measurements of Holtzman et al. (1995b) were taken with a gain of $14e^-$/DN and, hence, the correction that must be applied to the zero point is as shown in the above equation. The resulting STMAGs derived for the WFPC2 observations are listed in Table 6.

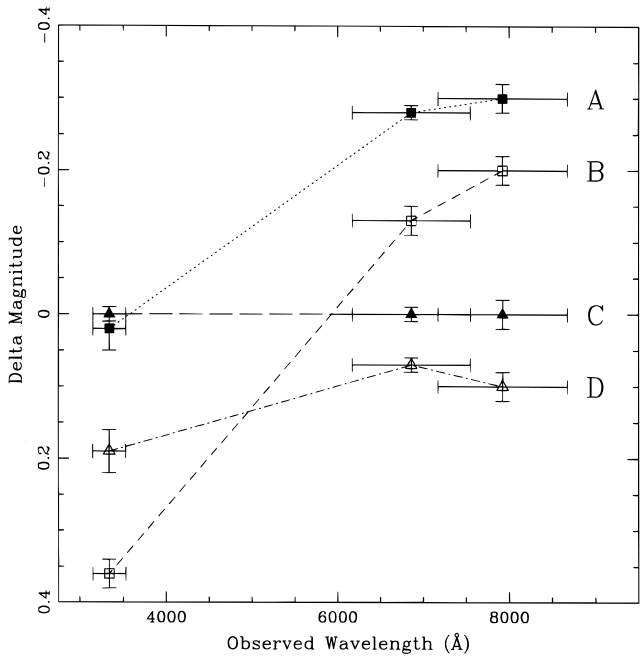

FIG. 3.—An illustration of the relative sight-line–dependent reddening in the Cloverleaf after applying an offset to shift the STMAGs of component C (the least reddened object) in the F336W, F702W, and F814W filters to zero. Details on the reddening, including the relative amplifications for some assumed models, are given in Table 8.

TABLE 6

APPARENT MAGNITUDES OF THE CLOVERLEAF AND ITS COMPONENTS

	STMAG						
COMPONENT	F555W[a] (1992.21)	F555W[a] (1992.33)	F555W[a] (1993.47)	F702W (1994.53)	F814W (1994.97)	F702W (1994.97)	F336W (1994.97)
Cloverleaf.....	16.71 (0.04)	16.89 (0.04)	16.68 (0.05)	17.14 (0.01)	17.35 (0.01)	17.08 (0.01)	17.64 (0.01)
A	18.04 (0.05)	18.18 (0.04)	17.91 (0.09)	18.44 (0.01)	18.66 (0.02)	18.40 (0.01)	19.03 (0.03)
B	18.21 (0.05)	18.41 (0.04)	18.22 (0.05)	18.61 (0.03)	18.76 (0.02)	18.55 (0.02)	19.37 (0.02)
C	18.27 (0.05)	18.43 (0.04)	18.26 (0.06)	18.75 (0.03)	18.96 (0.02)	18.68 (0.01)	19.01 (0.01)
D	18.35 (0.05)	18.61 (0.04)	18.40 (0.06)	18.85 (0.02)	19.06 (0.02)	18.75 (0.01)	19.20 (0.03)

[a] Based on results from the LUCY restoration method (Table 4). The errors (in parentheses) include errors from photometric calibration.

2.2.6. *Summary of Photometric Measurements*

We determined that the Cloverleaf's STMAG in WFPC F555W on 1992.21 was 16.71 ± 0.04 mag; it then decreased in brightness to 16.89 ± 0.04 mag by 1992.33 and increased in brightness to 16.68 ± 0.05 by 1993.47. Given the relative photometry reported in Table 4 for WFPC F555W, which we deem to represent the most reliable WFPC measurements, there is little evidence ($> 2\,\sigma \approx 0.06$ mag) for relative component brightness variations at the three WFPC epochs of observation.

The Cloverleaf's magnitude in WFPC2 F702W changed only slightly between the two WFPC2 epochs of observation. On 1994.53 it was 17.14 ± 0.01, and on 1994.97 it was 17.08 ± 0.01. There was also no significant change in the relative brightnesses of the four components through this filter at those two epochs (see Table 5). We determined the brightness of the Cloverleaf on 1994.97 through WFPC2 F814W to be 17.35 ± 0.01 and through F336W to be 17.64 ± 0.01.

2.3. *Searches for Additional Structure and the Lensing Object*

We used the 15 minute exposures through WFPC2 F702W to search for additional component structure and the lensing object. Figure 1 (*lower right*) shows the sum of the three 15 minute exposures. The contrast has been adjusted to reveal low surface brightness features. It is immediately apparent that components A and C are not perfect point sources but are elongated toward each other. This structure suggests the existence of an Einstein ring associated with the lens. The surface brightnesses at locations 1 and 2 in Figure 1 (*lower right*) are measured to be 19.3 and 19.7 mag arcsec^{-2}, respectively, in the STMAG system over regions that are ≈ 0.017 arcsec^2 in size (3 pixels $\times$ 3 pixels) in both cases. Kayser et al. (1990) identified additional structure in their radio image of the Cloverleaf. A stronger radio component was detected $\approx 0\farcs5$ north of component B (termed "SRS" by Kayser et al.). We determined that the surface brightness (again as measured in a box of size 3 pixels $\times$ 3 pixels) at the location of SRS (marked as location 4 in Fig. 1 [*lower right*]) to be 20.5 mag arcsec^{-2} in the STMAG system and adopt this as an upper limit since no feature was detected. Note that the PSFs of components B and D extend out to the position of SRS, which is why the upper limit here is rather poor. The surface brightness of the background is approximately 22.5 mag arcsec^{-2} (marked as location 5 in Fig. 1 [*lower right*]). Kayser et al. also noted that an apparent radio counterpart to component C was displaced $\approx 0\farcs2$ north of its optical position. Unfortunately, this is too close (within ≈ 5 pixels) to perform any type of sensitive reliable measurement given our knowledge of the PSF. Kayser et al. also identified extended radio structure between components A and B, but we find no evidence for an optical counterpart to this radio feature. The saturated cores of the four components in the long-exposure F702W images made it impossible to model suitable PSFs and reliably subtract out the components. Independent archival observations of saturated stars that could have been used to subtract out the point sources were inadequate.

Any lensing object which is expected to lie between the four components for the observed image morphology will require greater efforts to detect. Such an object could be quite large, extending to the region beyond the four components. We did the following to estimate the upper limit to the central surface brightness of any object hidden by the extended component PSFs near the center of the system. First, we assumed that the four components were perfect point sources and that the contribution of each of the sources to the brightness at the center would be equal to the brightness at a point diametrically opposite the center. Given the geometry of the system, any error in this assumption should have minimal effect since the components have similar brightnesses. The counts in a 5×5 pixel^2 box (corresponding to $0\farcs22$ on a side) were determined after background subtraction at each of five positions: the four outer corners and the center of the lens, defined to be $\approx 0\farcs5$ north and $\approx 0\farcs1$ east of component A (location 3 on Fig. 1 [*lower right*]). We found that the surface brightness at the center, after subtracting the four components, was 17 ± 15 counts per pixel, corresponding to a 1 σ detection of $m_{\rm F702W} \approx 21.8$ mag arcsec^{-2} in the STMAG system (i.e., an unreliable detection). We also determined the upper limit to the magnitude of a point source at the center of the lens. We used the PSF derived from a 100 s F702W image to add a point source to the summed 2700 s F702W image. The peak intensity of the artificial point source was set so that it could be detected at a 2 σ level of confidence, indicating that $m_{\rm F702W} > 22.7$ mag for any point source that is present. The measurements described in this section are summarized in Table 7.

3. CONSTRAINTS ON MODELS OF THE CLOVERLEAF

Two narrow absorption-line metal systems are seen in the spectra of the Cloverleaf components at $z_{\rm abs} = 1.438$ and $z_{\rm abs} = 1.660$ (Magain et al. 1988; Monier et al. 1997), and this has lead to the suspicion that the lens may be related to one or both objects. Assuming a redshift of

TABLE 7

WFPC2 F702W PHOTOMETRY AND LIMITS ON FAINT STRUCTURE IN THE CLOVERLEAF

Region Measured[a]	Object Type	STMAG F702W	Units
Location 1.....	Component A extension[b]	19.3	mag arsec^{-2}
Location 2.....	Component C extension[b]	19.7	mag arsec^{-2}
Location 3.....	Central region[c] — surface brightness	21.8[d]	mag arsec^{-2}
	Central region[c] — point source	>22.7	mag
Location 4.....	SRS[be]	>20.5	mag arsec^{-2}
Location 5.....	Background	22.5	mag arsec^{-2}

[a] See the text for details. Location numbers are marked on Fig. 1 (*lower right*).
[b] As measured in a 3 pixel × 3 pixel box (0.017 arcsec^2).
[c] Expected position of any lensing galaxy.
[d] 1 σ detection, taken as an upper limit.
[e] A stronger radio component termed "SRS" by Kayser et al. (1990), $\approx$0.″5 north of component B.

$z \approx 1.44$ for the lens, Kayser et al. (1990) developed two separate models for the lens: (1) two spherical galaxies with equal masses and (2) a single elliptical galaxy. These models differ in two important respects. First, the two-spherical-galaxies model differs from the single-elliptical-galaxy model by predicting a weak fifth component roughly near the optical centroid of the Cloverleaf. Second, the two-spherical-galaxies model predicts that components B and C should be more susceptible to microlensing effects and therefore more likely to vary, whereas the single elliptical model indicates components A and D should be more susceptible to microlensing. Both of the Kayser et al. models were able to adequately explain the *relative positions* derived from the radio and optical observations available at the time, but Kayser et al. (1990) did not favor one model over the other. Given the lack of a fifth component near the optical centroid of the Cloverleaf (§ 2.3), along with the observations reported by Arnould et al. (1993) and Remy et al. (1996) that indicate that components A and D can show more rapid variations than the others (we were unable to demonstrate this with the *HST* data), there is some evidence to favor the single-elliptical-galaxy model over the two-spherical-galaxies model.

Here we discuss how the observations provide better or new constraints on the relative astrometric positions of the image components (§ 3.1), the relative amplifications of the image components (§ 3.2), and limits on the brightness of any component structure and the lensing object, along with the lensing object's mass-to-light ratio given some reasonable assumptions (§ 3.3). Unfortunately, researchers interested in building models of the Cloverleaf must still make assumptions about the redshift of the lens.

3.1. *Astrometric Constraints*

From the series of six WFPC and 13 WFPC2 observations taken over the course of 2.76 yr at five epochs we have been able to achieve relative astrometric measurements accurate to $\approx$3 mas for the four components of this gravitationally lensed system (Table 2). With the exception of a 25 mas change in the relative declination of component D between the mean epoch of the WFPC and WFPC2 observations (see footnote to Table 2), there was no significant evidence for changes in the relative positions at the various epochs. Previous measurements by Magain et al. (1988) report accuracies of 20–30 mas, while a statistical error of 10 mas is inferred from results reported by Kayser et al. (1990). Thus, these new measurements are considerably more accurate and provide the primary and most reliable constraint on the lensing geometry.

3.2. *Dust Extinction Models and Derivation of the Relative Amplifications*

Given the lack of evidence for significant component-to-component brightness variations at the various *HST* observation epochs and the expected short time delays for brightness variations caused by slightly different path lengths along the four sight lines, we can safely assume that the observed relative magnitudes of the components are not adversely affected by time delays. Note that Kayser et al. (1990) predict that these should be less than 1 yr, and, in fact, Remy et al. (1996) have concluded from observations that the time delays are less than 1 month. However, because of the sight-line–dependent extinction, the observed relative magnitudes of the components in the optical are not representative of the relative amplifications. The WFPC2 F814W relative magnitudes are closest to the true relative amplifications; however, reasonable models suggest that even the extinction in this waveband is significant. If the dust giving rise to the sight-line–dependent extinction resides at approximately the QSO redshift, $z_{em} \approx 2.5$, then the F814W data corresponds to observations near $\approx$2300 Å in the rest frame of the dusty region. On the other hand, if the extinction resides near some of the metal-line redshifts, $z_{abs} \approx 1.44$–1.66, then this corresponds to observations near $\approx$3200 Å in the rest frame of the dusty region. In either case, even a moderate amount of dust can cause significant extinction at optical wavelengths. In order to explain the data reported in Table 5, we have considered four models for the dust extinction using extinction laws discussed by Cardelli, Clayton, & Mathis (1989) and Pei (1992). We assume that either the dust is Galactic-like or SMC-like and consider models with the dust at either $z \approx 2.5$ or $z \approx 1.5$. The estimates of dust extinction for the four models and the derived relative (extinction-corrected) amplifications are reported in Table 8. Consideration of the WFPC F555W relative magnitudes, which were taken at an earlier epoch, tend to favor SMC-like extinction over Galactic-type extinction at both redshifts. It should be emphasized that in deducing the results in Table 8 an extinction correction to component C has not been applied, since this would require information on the relative intrinsic spectral energy distribution of component C. Thus, any comprehensive lensing model for the Cloverleaf would have the freedom to adopt

TABLE 8

ESTIMATED EXTINCTIONS AND AMPLIFICATIONS RELATIVE TO COMPONENT C IN THE CLOVERLEAF[a]

Sight Line (Component)	A_{F336W} (mag)	A_{F555W} (mag)	A_{F702W} (mag)	A_{F814W} (mag)	A_J (mag)	A_H (mag)	A_K (mag)	Relative Amplifications
Results Assuming Galactic Extinction at $z_{ext} = 2.5$								
A.....	0.61	0.22	0.22	0.26	0.13	0.10	0.07	1.65
B.....	0.88	0.32	0.32	0.37	0.19	0.15	0.11	1.62
C.....	...	...	...	...	...	...	...	1.00
D	0.13	0.05	0.05	0.05	0.03	0.02	0.02	0.95[b]
Results Assuming SMC Extinction at $z_{ext} = 2.5$[c]								
A.....	0.63	0.38	0.28	0.24	0.15	0.11	0.07	1.68
B.....	0.87	0.53	0.39	0.34	0.20	0.15	0.10	1.61
C.....	...	...	...	...	...	...	...	1.00
D	0.13	0.08	0.06	0.05	0.03	0.02	0.02	0.95[b]
Results Assuming Galactic Extinction at $z_{ext} = 1.5$								
A.....	0.92	0.94	0.61	0.52	0.34	0.25	0.15	2.21
B.....	1.29	1.29	0.83	0.72	0.47	0.34	0.21	2.31
C.....	...	...	...	...	...	...	...	1.00
D	0.20	0.20	0.13	0.11	0.07	0.05	0.03	1.01[b]
Results Assuming SMC Extinction at $z_{ext} = 1.5$								
A.....	0.60	0.33	0.25	0.21	0.13	0.09	0.05	1.63
B.....	0.83	0.46	0.34	0.29	0.18	0.12	0.08	1.55
C.....	...	...	...	...	...	...	...	1.00
D	0.13	0.07	0.05	0.04	0.03	0.02	0.01	0.95[b]

[a] An extinction correction to component C itself has not been applied, since this would require knowledge of the relative intrinsic spectral energy distribution (see § 3.2).

[b] This value for the relative amplification of component D should be considered less reliable because of the possibility of microlensing (see § 4.1).

[c] Probably the most favored model because of better agreement with the earlier epoch WFPC F555W measurements and the detection of molecules at the redshift of the QSO.

an additional (but reasonable) constant extinction along all four sight lines.

It is also worth mentioning that another valuable constraint on the component amplifications can be derived from the emission-line spectra of the individual components. In particular, the broad emission lines in component D have smaller equivalent widths than those in components A, B, and C (Turnshek et al. 1997). This indicates that the ratio of the amplification of broad emission line region flux to continuum flux is smaller in component D than it is for components A, B, and C (which are nearly identical). This should prove to be an important additional constraint on the geometry required to produce the observed relative amplifications as well as the size scale of the emission-line region relative to the continuum-emitting region.

3.3. *Photometric Constraints and Lower Limits on the Mass-to-Light Ratio of a Single Lensing Galaxy*

In § 2.3, we discussed upper limits to the surface brightness of a lensing object located in between the four components. The data revealed an unreliable 1 σ detection of ≈ 21.8 mag arcsec^{-2} in the F702W filter. This corresponds to 28.5 mag pixel^{-2} on the PC (WFPC2 Instrument Handbook, Burrows et al. 1995). Assuming that this is the amount of light falling on the central pixel of the image of a giant elliptical galaxy at $z \approx 1.5$, the total integrated magnitude of the galaxy would be ≈ 4.9 mag brighter (Burrows et al. 1995), or $m_{F702W} \approx 23.6$ mag. Given the low level of confidence of any 1 σ detection, we will consider this an upper limit to the brightness of any lensing galaxy.

To produce an Einstein ring–like morphology (marginally observed) consistent with the angular size of the Cloverleaf, the mass of a lensing galaxy at $z \approx 1.5$ would be $\approx 1.6 \times 10^{11}\ M_\odot$ for $H_0 = 75$ km s^{-1} Mpc^{-1} and $q_0 = 0.5$. To derive a mass-to-light ratio that can be compared to ones derived for V-band observations of nearby ellipticals, we need to correct for the fact that observations in the F702W filter correspond to ≈ 2800 Å at redshift $z \approx 1.5$. However, the effects of evolution also need to be considered since nearby ellipticals are greater than 10 Gyr old, while the age of a galaxy at $z \approx 1.5$ could not exceed $\approx 3-4$ Gyr for a low H_0 value. The work of Bruzual & Charlot (1993) suggests that a color correction of approximately -3.8 mag between the F702W and V band would be typical for a 4 Gyr old elliptical; thus, the F702W observations can be taken as indirect evidence for a lensing galaxy that would have $V > 19.8$ mag. On the other hand, if the lensing galaxy were a 1 Gyr old elliptical with a bluer stellar population, the color correction would be only approximately -2.0 mag, and the F702W observation would suggest $V > 21.6$ for the lensing galaxy. (It should also be pointed out that an elliptical that was 4 Gyr old or older has close to minimum flux near 2800 Å, so sensitive measurements in the IR would be a much more effective way to search for the lensing galaxy.)

Having inferred limits on V from limits in the F702W filter, we would still like to consider what they imply for the minimum mass-to-light ratio of an elliptical-type lensing galaxy through comparison with results on nearby old ellipticals. The work of Bruzual & Charlot (1993) can again be used and suggests that $z \approx 1.5$ ellipticals of age 4 Gyr and 1

Gyr will decrease their brightnesses by ≈ 1 mag and ≈ 2 mag, respectively, as they evolve to the present epoch. Therefore, taking the combination of these effects into account, the relevant V-magnitude limits for comparison with mass-to-light ratios in nearby ellipticals are $V > 20.8$ mag (for the case where the assumed $z \approx 1.5$ lensing galaxy is 4 Gyr old) and $V > 23.6$ mag (for the case where the assumed $z \approx 1.5$ lensing galaxy is 1 Gyr old). Thus, the uncertainty for making a reasonable comparison is a factor of ≈ 13. Adopting these values (again for $H_0 = 75$ km s^{-1} Mpc^{-1} and $q_0 = 0.5$) we find a V-band $M/L > 0.7\ M_\odot/L_\odot$ (4 Gyr old, $z \approx 1.5$ galaxy) and $10\ M_\odot/L_\odot$ (1 Gyr old, $z \approx 1.5$ galaxy). Thus, our inability to find significant evidence for the lensing galaxy is not surprising since V-band mass-to-light ratios for nearby ellipticals lie in the range of $\approx 10-20\ M_\odot/L_\odot$ (Lauer 1985; Binney & Tremaine 1987). A more serious problem would have been encountered if we had assumed that the lensing galaxy was a spiral type, because the rest frame f_λ flux at ≈ 2800 Å in a young spiral would be larger or comparable to the flux in the V band. Using the same type of reasoning as before, the F702W limits could be used to indirectly infer that $M/L > 30\ M_\odot/L_\odot$, which is uncharacteristic of nearby spirals.

In summary, for $H_0 = 75$ km s^{-1} Mpc^{-1} and $q_0 = 0.5$, we conclude that if the lensing galaxy is near $z \approx 1.5$, it is likely a young (1–4 Gyr) elliptical $1.6 \times 10^{11}\ M_\odot$. This is consistent with the nondetection of the lensing galaxy. Any dust associated with such a lensing galaxy would probably be SMC-like rather than like dust found in the Galaxy.

4. SUMMARY AND DISCUSSION

The results of this *HST* WFPC/WFPC2 imaging investigation of the gravitationally lensed Cloverleaf BAL QSO H1413+1143 can be summarized as follows:

4.1. *Astrometry*

Through a series of observations we have been able to achieve relative astrometric measurements accurate to ≈ 3 mas for the four components of this gravitationally lensed system (Table 2, but also see the footnote). This is a factor of 3 better than the statistical errors inferred from the best previous results.

4.2. *Photometry*

We have obtained photometric measurements over a time baseline spanning 2.76 yr in the observed frame (≈ 1.09 yr proper time in the QSO rest frame) at five different epochs using several different filters. The results (Tables 2–5) show no significant evidence for relative component-to-component brightness variations at the various epochs. Table 6 gives measured apparent magnitudes in the STMAG system.

4.3. *Sight-Line–dependent Extinction*

The derivation of WFPC2 F336W–F814W color indices for the components (Table 5) reveal the presence of sight-line–dependent extinction. Component B (the most reddened) is 0.56 ± 0.04 mag redder than component C (the least reddened). We considered four dust extinction models to explain this reddening (§ 3.2, Table 8).

The location of the sight-line–dependent extinction remains unclear; the possibilities include extinction arising in: the lensing galaxy, one of the intervening absorbers (which may be associated with the lensing galaxy), the QSO host galaxy, or the QSO BAL region. Results from the *HST* Faint Object Spectrograph (FOS) component spectroscopy of H1413+1143 are reported in Monier et al. (1997), who consider constraints that can be placed on cosmologically intervening absorbers, and Turnshek (1995) and Turnshek et al. (1997), who consider constraints that can be placed on the BAL region clouds.

The unambiguous discovery of dust in cosmologically intervening absorbers would be very significant. This would be firm evidence for obscuration in the universe that could be pervasive at higher redshifts. Fall & Pei (1993 and references therein) have considered this question in the context of damped Lyα absorption systems, but clearly their discussion could be extended since some of the weak metal-line systems in H1413+1143 might be low column density damped systems.

Recently, Webster et al. (1995) claimed that a majority of QSOs might be hidden because of significant amounts of dust obscuration, based on observations of a sample of flat-spectrum radio sources. This claim has been challenged by Boyle & Di Matteo (1995), but their X-ray selected sample still permits up to 2 mag of extinction in the B band. Barvainis et al. (1995) compared the spectral energy distribution of H1413+1143 with the dusty source IRAS FSC 10214+4724, which evidently is also a lensed object (see § 4.6 below), and estimated $A_V \approx 0.5$ mag for it.

Turnshek et al. (1994), Sprayberry & Foltz (1992), and Weymann et al. (1991) have recently considered the question of dust along directions toward BAL QSOs, and there is good evidence for SMC-like dust in some objects. The so-called low-ionization BAL QSOs are the objects that exhibit most of the evidence for dust, but PG0043+039, which shows only weak high-ionization BALs, seems to exhibit similar evidence. Given that Barvainis et al. (1994) find CO emission at the redshift of H1413+1143, the QSO redshift should probably be considered the most likely location of the dust. On the other hand, most BAL QSOs do not show evidence for dust, so the other models should not be completely ruled out. The discovery of a number of low-ionization atomic and molecular lines at the redshift of the QSO shows that there may be 10^{10}–$10^{11}\ M_\odot$ of cool material within 2–3 kpc of the nucleus (Barvainis 1995; Barvainis et al. 1994; Wilner, Zhao, & Ho 1995). These data therefore lend weight to the possibility that the dust is located at the QSO redshift.

4.4. *Relative Amplifications*

Sight-line–dependent extinction is clearly present in the Cloverleaf, and this has to be modeled to infer the actual relative component amplifications. On the other hand, at the different *HST* observation epochs we do not find significant evidence for changes in relative component brightnesses. Evidently, time delays along the sight lines are short enough (or intrinsic brightness variations small enough) that changes in relative component brightnesses are not easily detected. However, while not apparent from the *HST* observations, the light curve of component D has been reported to show quantitatively different variations with respect to the other components (Remy et al. 1996), and our FOS spectra show smaller equivalent widths for the emission lines in this component (see § 3.2 and Turnshek et al. 1997). Furthermore, the flux ratios of components A, B, and

C obtained from the *HST* F702W and F814W observations are nearly identical to the *R*- and *I*-band observations reported by Kayser et al. (1990) (they are the same to within an accuracy of a few percent, which is probably indicative of the observational errors), but component D is significantly brighter (by $\approx 19\%$) at the *HST* observation epochs. It is therefore plausible that microlensing is important for component D, and so the derived magnification factor for component D should be considered with some caution.

We simultaneously determined the relative magnifications and extinctions along each sight line relative to component C for four possible combinations of Galactic or SMC-like extinction at two redshifts (see § 3.2 and Table 8). None of the derived results on relative amplifications are consistent with the Kayser et al. (1990) gravitational lens models of the Cloverleaf. It should be kept in mind, however, that Kayser et al. did not seriously consider observational constraints on amplifications because of the possible importance of time delays or microlensing. Based on our new work, it is clear now that accounting for the effects of sight-line–dependent extinction is the most important consideration. The new results on component amplifications represent new and reliable constraints on the Cloverleaf, with SMC-like dust at $z \approx 2.5$ probably representing the most likely extinction model (see previous subsection). We note that the model for intervening Galactic-type extinction leads to the prediction that component C should be the brightest component in the F555W image, at odds with our observations. This extinction model can therefore probably be excluded from further consideration.

4.5. *The Lensing Galaxy and Component Structure*

We did not find any significant evidence for the lensing object but did identify some evidence for extended structure associated with components A and C that might be part of an Einstein ring. We set photometric brightness limits (see Table 7) at the expected position of any lensing galaxy and at the positions of weak radio sources observed by Kayser et al. (1990). By assuming a simple model for a lensing galaxy at redshift $z \approx 1.5$ we were able to place constraints on the mass-to-light ratio of the lensing galaxy (§ 3.3).

The most sensitive results from the existing data have come from the grand total of 55 minutes of exposure with the WFPC2 F702W filter. With the "dithering" observing technique now recommended by Space Telescope Science Institute, these data could be improved on, and we might go ≈ 1 mag fainter with more accurate PSF subtraction. If a candidate for the lensing galaxy still remained (essentially) undetected, it would begin to raise the mass-to-light ratio of the lensing object to an interesting value. At the same time, while the QSO itself may be the most likely site for the dust extinction, it still cannot be ruled out that the extinction occurs in a foreground object (e.g., the lensing galaxy) and that the lensing galaxy itself suffers from significant extinction. Given the current brightness limit, directly determining the redshift of the lensing object from spectral features in the near future will be extremely difficult, since there is barely a hint of a candidate for the lens in the existing WFPC2 data.

It may be of interest to note that models of the Cloverleaf by Kochanek (1992) in an Einstein–de Sitter universe with zero cosmological constant predict the most probable lens redshifts to be 0.68 ± 0.33 and 0.92 ± 0.40 for the two lens velocity dispersions that were considered. The lensing galaxy at these redshifts is predicted to be fainter than component D by ≈ 4 mag in the *R* band, which would be ≈ 22.8 mag on the F702W STMAG system. This is ≈ 0.8 mag brighter than the upper limit of ≈ 23.6 given in § 3.3 but is still not easily detected given the background measurement error. However, the lens redshift probability distributions for models with a non zero cosmological constant peak at or near the absorption line redshifts of 1.44 and 1.66. In these models the lensing galaxy is predicted to be fainter than component D by at least 6 mag in the *R* band, i.e., ≈ 25 mag.

4.6. *H1413+1143: Not an Intrinsically Unique Object?*

Aside from the fact that H1413+1143 is gravitationally lensed, the object appears to be unique in other ways. Not only is the object a BAL QSO, but some rare BAL features are present, including P V and Al III (Turnshek et al. 1987, 1988, 1997). Also, H1413+1143 is one of a subset of BAL QSOs that is known to have significant optical polarization, in this case $\approx 4\%$ (Goodrich & Miller 1995; Cohen et al. 1995). Finally, as noted earlier, H1413+1143 was recently found to be one of a few high-redshift strong CO emitters (Barvainis et al. 1994). In this respect, it is interesting that the prototypical ultraluminous IRAS galaxy, FSC 10214+4724, which is also known for its strong CO emission, has recently been recognized as a gravitationally lensed system (Broadhurst & Lehar 1995; Eisenhardt et al. 1996). The amplification aspects of gravitational lensing evidently contribute to these CO detections. It may be that some of these properties are related, e.g., the presence of BALs along with molecules and dust in some cases. This makes regions residing within the QSO host galaxy itself (not necessarily the BAL region) good candidates for the site of the dusty region. Why should these objects, which are thought to be rather peculiar and rare, show up as gravitationally lensed systems? Maybe they are common objects but at significantly lower luminosity after amplification effects are taken into account.

Despite the current difficulties associated with identifying the lensing galaxy, it is clear that the Cloverleaf should be widely recognized as providing unique opportunities to study a number of cosmologically important phenomena. Of interest for future study will be cosmological parameters, the mass-to-light ratio and properties of the lensing galaxy, cross sections and kinematics of intervening absorbers, and constraints on the broad emission and broad absorption line regions. Future IR imaging observations at long enough wavelengths would allow the dust-extinction models to be evaluated and permit a more direct measurement of the relative component amplifications.

We wish to thank V. Khersonsky, S. Casertano, and C. Hazard for helpful discussions during the course of this work, K. Chae for his work on lens models of the Cloverleaf, and S. Sherer for assistance. This work was based on observations made with the NASA/ESA *Hubble Space Telescope*, operated by AURA under NASA contract NAS 5-26555. C. Sirola acknowledges partial support from the Zaccheus Daniel Fellowship during some phases of this work.

REFERENCES

Angonin, M., Vanderriest, C., & Surdej, J. 1990, in Gravitational Lensing, ed. Y. Mellier, B. Fort, & G. Soucail (Lecture Notes in Physics, 360; Berlin: Springer), 124
Arnould, P., et al. 1993, in Proceedings of the 31st Liege International Astrophysical Colloquium, Gravitational Lenses in the Universe, ed. J. Surdej et al. (Liege: Univ. Liege, Inst. d'Astrophys), 169
Barvainis, R. 1995, BAAS, 27, 871
Barvainis, R., Antonucci, R., Hurt, T., Coleman, P., & Reuter, H.-P. 1995, ApJ, 451, L9
Barvainis, R., Tacconi, L., Antonucci, R., Alloin, D., & Coleman, P. 1994, Nature, 371, 586
Binney, J., & Tremaine, S. 1987, Galactic Dynamics (Princeton: Princeton Univ. Press)
Boyle, B., & Di Matteo, T. 1995, MNRAS, 277, L63
Broadhurst, T., & Lehar, J. 1996, ApJ, 450, L41
Bruzual, A., & Charlot, S. 1993, ApJ, 405, 538
Burrows, C., et al. 1995, WFPC2 Instrument Handbook (Baltimore: STScI)
Cardelli, J., Clayton, G., & Mathis, J. 1989, ApJ, 345, 245
Cohen, M., et al. 1995, ApJ, 448, L7
Drew, J., & Boksenberg, A. 1984, MNRAS, 211, 813
Eisenhardt, P., et al. 1996, ApJ, 461, 72
Falco, E. 1993, in Proceedings of the 31st Liege International Astrophysical Colloquium, Gravitational Lenses in the Universe, ed. J. Surdej, et al. (Liege: Univ. Liege, Inst. d'Astrophys.), 127
Fall, S. M., & Pei, Y. C. 1993, ApJ, 402, 479
Goodrich, M., & Miller, J. 1995, ApJ, 448, L3
Hazard, C., Morton, D. C., Terlevich, R., & McMahon, R. 1984, ApJ, 282, 33
Holtzman, J. A., et al. 1995a, PASP, 107, 156
———. 1995b, PASP, 107, 1065
Houde, M., & Racine, R. 1994, AJ, 107, 466
Hutsemekers, D. 1993, A&A, 280, 435
Kayser, R., Surdej, J., Condon, J., Kellerman, K., Magain, P., Remy, M., & Smette, A. 1990, ApJ, 364, 15
Kochanek, C. S. 1992, ApJ, 384, 1
Krist, J. 1993, in ASP Conf. Ser. 52, Proc. 2d Astronomical Data Analysis Software and Systems Conference, ed. R. J. Hanish, R. J. V. Brissenden, & J. Barnes (San Francisco: ASP), 536
Lauer, T. 1985, ApJ, 292, 104
Lucy, L. 1971, ApJ, 163, 95
Magain, P., Surdej, J., Swings, J.-P., Borgeest, U., Kayser, R., Kuhr, H., Refsdal, S., & Remy, M. 1988, Nature, 334, 325
Monier, E., Turnshek, D. A., & Lupie, O. L. 1997, ApJ, submitted
Pei, Y. 1992, ApJ, 395, 130
Phillips, A. C., Forbes, D. A., Bershady, M. A., Illingworth, G. D., & Koo, D. C. 1994, AJ, 107, 1904
Remy, M., Gosset, E., Hutsemekers, D., Revenaz, B., & Surdej, J. 1996, in IAU Symp. 173, Astrophysical Applications of Gravitational Lensing, ed. C. Kochanek & J. Hewitt (Dordrecht: Kluwer), 261
Saust, A. B. 1994, A&AS, 103, 99
Sprayberry, D., & Foltz, C. B. 1992, ApJ, 390, 39
Smette, A., Robertson, J. G., Shaver, P. A., Reimers, D., Wisotzki, L., & Kohler, Th. 1995, A&AS, 113, 199
Surdej, J. 1990, in Gravitational Lensing, ed. Y. Mellier, B. Fort, & G. Soucail (Lecture Notes in Physics, 360; Berlin: Springer), 57
Turnshek, D. A., Briggs, F. H., Foltz, C. B., Grillmair, C. J., & Weymann, R. J. 1987, in QSO Absorption Lines: Probing the Universe (Poster Papers), ed. J. C. Blades, C. Norman, & D. A. Turnshek (Baltimore: STScI), 8
Turnshek, D. A., Foltz, C. B., Grillmair, C. J., & Weymann, R. J. 1988, ApJ, 325, 651
Turnshek, D. A. 1988, in QSO Absorption Lines: Probing the Universe, ed. J. C. Blades, D. A. Turnshek, & C. Norman (Cambridge: Cambridge Univ. Press), 17
———. 1995, in QSO Absorption Lines: An ESO Workshop Held 21–24 November 1994, ed. G. Meylan (Berlin: Springer), 223
Turnshek, D. A., et al., 1994, ApJ, 428, 93
Turnshek, D. A., Lupie, O. L., Monier, E., Sirola, C., & Espey, B. R. 1997, in preparation
Webster, R., Francis, P., Peterson, B. A., Drinkwater, M., & Masci, F. 1995, Nature, 375, 469
Weymann, R. J. 1995, in QSO Absorption Lines: An ESO Workshop Held 21–24 November 1994, ed. G. Meylan (Berlin: Springer), 213
Weymann, R. J., Turnshek, D. A., & Christiansen, W. 1985, in Astrophysics of Active Galaxies and Quasi-stellar Objects, ed. J. Miller (Mill Valley: Univ. Science Books), 333
Weymann, R. J., et al. 1991, ApJ, 373, 23
Whitmore, B. 1995, in Calibrating *Hubble Space Telescope* Post Servicing Mission, ed. A. Koratkar & C. Leitherer (Baltimore: STScI), 269
Wilner, D. J., Zhao J. -H., & Ho, P. T. P. 1995, ApJ, 453, L91